Tellus SERIES A DYNAMIC METEOROLOGY AND OCEANOGRAPHY
PUBLISHED BY THE INTERNATIONAL METEOROLOGICAL INSTITUTE IN STOCKHOLM

Remote effects of tropical cyclones on heavy rainfall over the Korean peninsula – statistical and composite analysis

By KUN-YOUNG BYUN* AND TAE-YOUNG LEE, *Global Environment Laboratory and Department of Atmospheric Sciences, Yonsei University, 134 Shinchon-Dong, Seodaemun-Gu, Seoul 120-749, Korea*

(Manuscript received 15 April 2011; in final form 13 November 2011)

ABSTRACT

This study investigates the remote effects of tropical cyclones (TCs) on heavy rainfall (HR) over the Korean peninsula through statistical and composite analyses for 1981–2009. Statistical analysis indicates that the 29-year mean annual rainfall occurring with TCs within 3000 km of Korea is 658 mm, 49% of the 29-year total mean annual rainfall of 1340 mm. About 32% of the total mean annual amount occurs with TCs within the range of 1200–2800 km. The probability of HR over the peninsula is higher with TCs that make landfall on southern and eastern China compared to other regions. In the HR composite, the synoptic-scale pressure pattern during the remote TC events is characterised by a synoptic-scale trough to the northwest, a western Pacific subtropical high (WPSH) to the southeast and a TC to the southwest of the Korean peninsula. This pattern results in a region of strong rising motion located beneath the upper-level jet (ULJ) entrance region, concurrent with a region of convective instability enhanced by strong moisture transport and quasi-geostrophic (QG) forcing for ascent by warm-air advection. The composite analysis shows that remote TCs can influence HR over the peninsula by helping to establish a convectively unstable environment and a large-scale convergence of air.

Keywords: remote effects, tropical cyclones, heavy rainfall, statistical analysis, composite analysis

1. Introduction

A tropical cyclone (TC) is a storm system characterised by a low-pressure centre and numerous thunderstorms that produce strong winds and heavy rainfall (HR). One of the primary hazards caused by TCs is post-landfall HR and attendant freshwater flooding (American Meteorological Society [AMS], 2007). A TC can produce tremendous rainfall in its eyewall and its surrounding rainbands. This rainfall is generally referred to as the direct effect of TC on precipitation, or precipitation associated with the TC vortex itself (Wang et al., 2009).

A TC can also induce HR at large distances from the TC vortex itself when it interacts with other mid-latitude synoptic systems (Wang et al., 2009). These increases in rainfall in areas far away from the TC are generally referred to as remote, distant, or indirect effects of a TC on precipitation (Bosart and Carr, 1978; Ross and Kurihara, 1995; Chen et al., 2006; Schumacher et al., 2011).

Pierce (1939) was probably the first to study a major rainfall event caused by the remote effects of the historic New England TC during September 17–21, 1938. Bosart and Carr (1978) presented a detailed analysis of the remote effects of Hurricane Agnes (1972). They showed that the northeastern area far from the centre of the TC had the potential for flooding, due to both convergence by a weak short-wave and plentiful moisture from the TC's circulation. Recently, Cote (2007) defined the term predecessor rain event (PRE) to describe meso- and subsynoptic-scale regions of high-impact HR that occurred well in advance of TCs over the eastern US (Galarneau et al., 2010). Galarneau et al. (2010) presented the conceptual model of the synoptic-scale environment associated with PREs in advance of TCs with anticyclonically curved upper-level jets (ULJs). Galarneau et al. (2010) showed that on the synoptic-scale, PREs form in the equatorward jet-entrance region of a 200-hPa jet on the western flank of a 925-hPa equivalent potential temperature ridge located east of a 700-hPa trough. On the mesoscale, PREs occur in conjunction with low-level frontogenetical forcing along a baroclinic zone where HR is focused.

*Corresponding author.
email: buildg@yonsei.ac.kr

Citation: Tellus A 2012, **64**, 14983, DOI: 10.3402/tellusa.v64i0.14983

Schumacher et al. (2011) quantified the effects of the tropical moisture from TC Erin on a high-impact PRE.

The occurrence of HR induced by remote TCs is not limited to TCs originating over the eastern US. Higgins and Shi (2005) examined the relationships between Gulf of California moisture surges and TCs in the eastern Pacific basin. Farfán and Fogel (2007) investigated the influence of TC circulations in the distribution of humidity a nd convection over northwestern Mexico. Recent studies (Corbosiero et al., 2009; Ritchie et al., 2011) explored the role of eastern North Pacific TCs and their remnants on southwestern US rainfall events. Waylen and Harrison (2005) provided a useful methodology for examining the remote effects of TCs on the daily rainfall record in the Caribbean basins. These researchers showed that precipitation falling in coincidence with the passage of TCs accounts for approximately 15% of the average annual precipitation in Liberia, Costa Rica. Stohl et al. (2008) found that the transport of tropical and subtropical moisture associated with two former TCs triggered an extreme precipitation event on the Norwegian southwest coast. Murata (2009) found that TC Meari (2004) resulted in HR along the Kii peninsula in Japan, which was located more than 500 km away from the typhoon center. Western North Pacific TC Songda (2004) enhanced remote precipitation in Japan, mainly through northward moisture transport by the TC's outer circulation into the preconditioned local precipitation system (Wang et al., 2009).

There have been several case studies of HR over Korea associated with remote TCs (Park et al., 1986; Sun and Lee, 2002; Shim and Hong, 2003; Kim, 2004; Shin and Lee, 2005; Lee, 2008; Hong and Lee, 2009). Park et al. (1986) investigated synoptic-scale features of a HR event over the Korean peninsula that occurred in association with the landfall of a tropical depression (TD), June (1984) over southern China. Park et al. (1986) showed that the HR over Korea formed within an area of synoptic-scale intrusion of tropical air from southern China into Korea along the surface front. Lee and Kim (2007) demonstrated that one type of environment producing heavy precipitation systems over Korea occurs when a typhoon makes landfall on the southeastern coast of China. Kim (2004) showed that 70% of HR events with daily rainfall amounts over 350 mm were accompanied by landfalling TCs in southern China. According to these previous studies, TCs in southern China are generally understood as important factors for the formation of HR over the Korean peninsula. However, detailed statistical or composite analysis focusing on the relationships between remote TCs and HR over the Korean peninsula has not been made.

The frequent occurrence of HR over the Korean peninsula during summer is strongly influenced by synoptic-scale features. Common large-scale features for HR are the presence of the western Pacific subtropical high (WPSH) and strong low-level southwesterlies (or jets) over the northwestern edge of the WPSH (Lee and Kim, 2007; Ninomiya and Akiyama, 1992). The poleward transport of warm, moist tropical air toward the Korean peninsula by the low-level southwesterly flow is important for the development of HR over the peninsula (Hong, 1992; Hwang and Lee, 1993; Lee et al., 1998; Sun and Lee, 2002). It is yet to be studied how remote TCs can provide a favorable environment for HR over the Korean peninsula through interaction with the abovementioned surrounding environments.

The purpose of this paper is to examine the climatology and typical environments associated with heavy precipitation over the Korean peninsula occurring with remote TCs. We attempt to understand the relationships between remote TCs and HR over the Korean peninsula using both statistical and composite analyses.

This paper is organised in the following manner. Section 2 describes the data and methods used in this study. In Section 3, climatology and statistical analysis on the relationships between remote TCs and HR over the Korean peninsula are presented. Section 4 shows composite analysis, including synoptic environments, and the relationship between heavy precipitation and remote TCs. Finally, a summary and conclusions are provided in Section 5.

2. Data and methods

Heavy rainfall cases are selected based on the observed precipitation data from about 70 manned stations of the Korea Meteorological Administration (KMA). The criterion for HR in this study is $\geq$40 mm (6 h)$^{-1}$ for at least one station and a total-station averaged amount $\geq$5 mm (6 h)$^{-1}$. The value of 40 mm (6 h)$^{-1}$ is based on the heavy rain advisory ($\geq$80 mm [12 h]$^{-1}$) of the KMA, and the station-averaged rainfall criterion is adopted to exclude isolated heavy rain events. This paper uses TC best-track data for 1981–2009 archived by the Regional Specialised Meteorological Centers (RSMC) – Tokyo Typhoon Center (http://www.jma.go.jp/jma/jma-eng/jma-center/rsmc-hp-pub-eg/trackarchives.html). The data include names, positions (in latitude and longitude), grades, central pressures, maximum sustained wind speeds and radii of 30-knot (15.4-m s^{-1}) winds and 50-knot (25.7-m s^{-1}) winds in 6-h intervals.

Galarneau et al. (2010) defined the PRE based on a clear separation on the radar imagery and the advection of tropical moisture from a TC. However, there are no radar data over the ocean. In this study, rainfall outside of the critical radius, which varies with TCs, is defined as remote

rainfall. Nakano et al. (2010) defined the critical radius as 300 km from the centre of each typhoon. This study considers the TC size and excludes the mixed (direct and remote) effects of TC on precipitation. The critical radius is calculated as the sum of the following three values: (1) the longest radius of 15.4-m s^{-1} winds provided by RSMC; (2) the maximum distance from the radius to the rain fields induced by the TC itself; and (3) the 6-hourly moving distance of TCs (Fig. 4b). The RSMC provides the radii of 30-knot (15.4-m s^{-1}) winds and 50-knot (25.7-m s^{-1}) winds except for TDs, and this study has used the radius of the tropical storm or typhoon at the nearest time for the radius of TD. Matyas (2010) presented that the edge of the rain fields in the northeast and northwest quadrants tended to be 50–75 km in front of the radius of 17 m s^{-1} winds. The mean 6-hourly moving distance of TCs over 29 yr is 1.1° with a standard deviation of 0.65°. This study has adopted 100 km (>50–75 km) for the maximum distance from the radius to the rain field and 194.25 km (~1.75°) for the 6-hourly moving distance of TCs. The critical radius is dependent on the longest radius of 15.4 m s^{-1} winds provided by the RSMC. The minimum radius of 15.4 m s^{-1} winds among TCs around the Korean peninsula is approximately 58 km (30 nautical miles). The minimum critical radius (350 km) is larger than the 300 km radius of Nakano et al. (2010) but smaller than the 410 km of minimum separation distance of Galarneau et al. (2010). In this paper, advection of tropical moisture from remote TCs is confirmed by checking the moisture flux and wind fields in the 850–700 hPa layer plotted on horizontal maps.

This study has utilised the method proposed by Waylen and Harrison (2005) for examining the relationships between the frequency of HR events and the distance and direction of remote TCs. The statistical analysis of Ho et al. (2004) is also used in this study to examine how the locations of TCs affect the incidence of HR events. To obtain the relationships between rainfall amounts over the peninsula and typhoon location, each 6-hourly typhoon position is binned into 2.5° latitude–longitude grid boxes.

For a detailed analysis of time evolution of the synoptic fields, the composite analyses have been generated using 1.25° × 1.25° gridded Japanese 25-year reanalysis (JRA-25) data (Onogi et al., 2007). The compositing method has had a long and successful history in TC research (Frank, 1977; McBride and Zehr, 1981; Camargo and Sobel, 2004) and has been used in recent studies on HR related to TCs (Higgins and Shi, 2005; Atallah et al., 2007; Milrad et al., 2009). Composite analysis does not capture potentially important characteristics of individual storms; however, it retains signatures that appear repeatedly (Hanley et al., 2001). A composite study is a useful method for examining the similarities and differences in the synoptic-scale atmospheric structure between HR and no rainfall (NR) events for a given location of TCs. The HR composite is divided into TCs making landfall in China (LT composite) and TCs over the ocean (e.g. the East China Sea, OT composite). The composite analyses are made using the 6-hourly JRA-25 data at the analysis time immediately before HR initiation (T − 0), 48 and 24 h prior to T − 0 (T − 48, T − 24), and 24 and 48 h after T − 0 (T + 24, T + 48). Heavy rainfall initiation time is defined as the time when HR begins after a period of no HR in the past 48 h. For NR cases, the middle time among the zero-rainfall period in each case was chosen.

3. Statistical relationships between remote TCs and HR over South Korea

Statistical analysis has been conducted to determine the location of TCs that are favorable for remote rainfall over the Korean peninsula. Figure 1a shows the frequency of

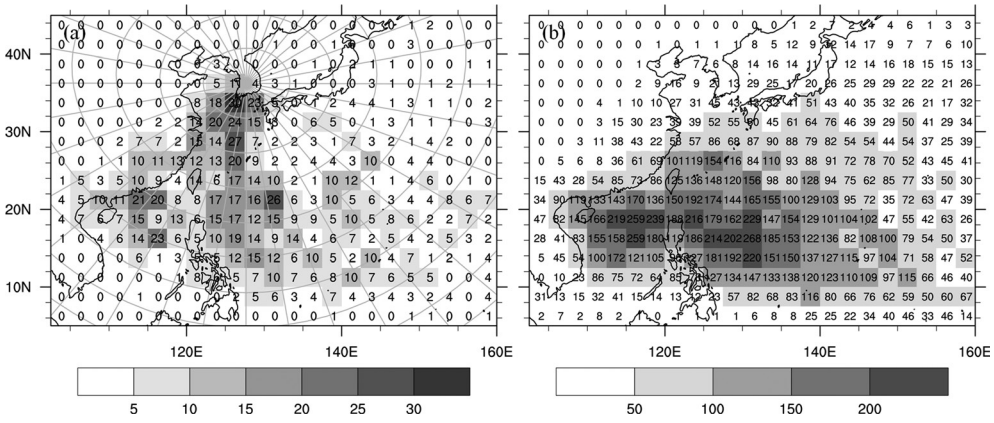

Fig. 1. (a) Frequency of HR over the Korean peninsula that occurred with the tropical cyclones (TCs) in each grid box. When multiple TCs are present, only the nearest TC is considered. (b) Geographical distribution of typhoon passage frequency for 1981–2009.

HR over the Korean peninsula that occurred with TCs located in each grid box over 29 yr (1981–2009). Heavy rainfall occurred frequently over the Korean peninsula when a TC passed over the South China Sea, the East China Sea, the Philippine Sea and China. However, this finding does not necessarily mean that TCs over those locations could more effectively induce remote HR over Korea because more typhoons pass over the South China Sea and the Philippine Sea (Fig. 1b).

Figure 2 shows the relationship between the mean annual amount of rainfall over South Korea and the distance or direction of TCs for the 29-year period. The method proposed by Waylen and Harrison (2005) is used to separate the annual amount of rainfall occurring with TCs as a function of distance of the nearest TC from the median station (36° 15′N, 127° 44′E) in South Korea (Fig. 2a). The median station is determined by the median longitude and median latitude value of all stations. The mean annual amount in Fig. 2 is the 29-year average of the total rainfall amount during all recorded time points with TCs at a certain distance range (or direction). The largest amount of rainfall occurs mainly when TCs are in the distance range of 1800–2400 km and in the direction range of 180–200°. Rainfalls with TCs closer than about 700 km may be interpreted as the amount directly produced by TCs. The peak amount of this direct effect is found at a distance of 400–600 km from the median station.

The mean accumulated amount of rainfall occurring with TCs within 3000 km distance is 658 mm (Fig. 2a), accounting for 49% of the mean annual total rainfall amount of 1340 mm (average amount for the 29-year period 1981–2009). The figure also indicates that about 32% of the mean annual total amount occurs with TCs in the distance range of 1200–2800 km. It can be said that remote TCs are an important element of a favorable environment for HR around the Korean peninsula during summer.

Most HRs during the TC events are found when TCs are within the direction range of 120–220° (Fig. 2b). In addition, most direct TC rainfalls are found with TCs to the south (180°) of the peninsula.

To find the location of the remote TC that can be related to the corresponding HR over the Korean peninsula, this study utilised the TC location from the RSMC data and observed precipitation data. Figure 3a shows 6-hourly average precipitation for the last 29 yr over South Korea for periods with TCs located in each grid box. TCs in the vicinity of the Korean peninsula directly produce large amounts of rainfall. Significant amounts of rainfall also occur frequently over Korea at the same time that TCs over southern and eastern China make landfall and TCs pass over the East China Sea. Figure 3b shows the percentage of TCs that are accompanied by HR over the Korean peninsula as selected from among the entire set of TCs located within the analysis grid over the 29-year study period. In this figure, events having a direct TC effect are excluded using the concept of the critical radius of the TC. This figure indicates that certain specific locations for remote TCs are associated with a higher probability (10–20% along the coast, 14–36% on the inland of southern China) of HR over the Korean peninsula, thereby agreeing with previous case studies which explained the role of the TC in southern China as a factor in HR over the Korean peninsula (Park et al., 1986; Kim, 2004). When TCs are over Taiwan and the southern East China Sea, the likelihood of HR over the peninsula increases by approximately 10%. Based on this result, composite analysis is carried out for cases of TC within the box area (20–30°N, 107.5–132.5°E) as in Fig. 3b.

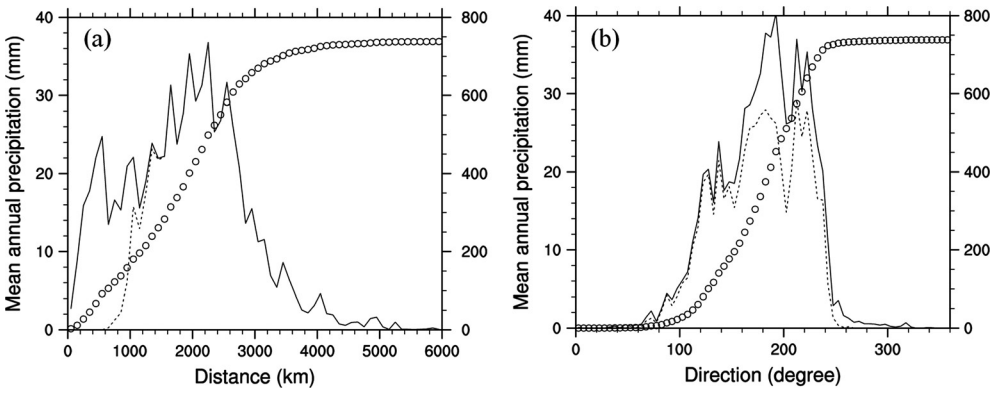

Fig. 2. Mean annual amount of rainfall occurring with TCs (solid line) as a function of: (a) distance (every 100 km); and (b) direction (every 5°) of TC from the median station (36° 15′N, 127° 44′E) in South Korea for 1981–2009. Its accumulation with the distance or the direction is represented by the line of open circles. Dotted line is for the mean annual amount excluding the rainfall cases with TCs inside of the critical radius, which is defined in the text.

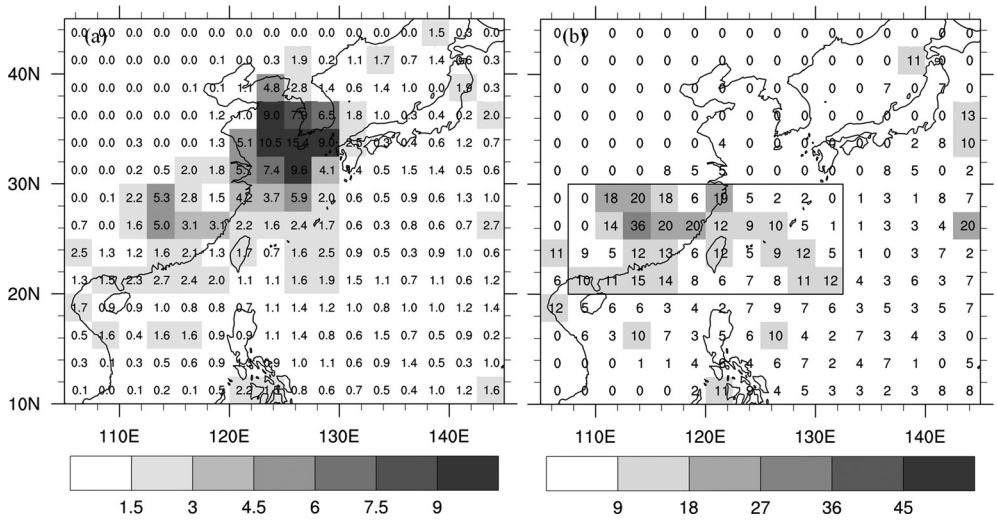

Fig. 3. (a) Six-hour precipitation amount averaged over South Korea and over the events with TCs passing through $2.5^\circ \times 2.5^\circ$ grid; and (b) the percentage of TCs that were accompanied with HR over the Korean peninsula, among the whole TCs that were located within each grid for 29 yr (1981–2009). In (b), events of direct TC effect are excluded using the concept of critical radius of TC (explanation is given in the text), and the box region (20–30°N, 107.5–132.5°E) is the area of remote TC for composite analysis.

Tracks of TCs over the western Pacific are predominantly controlled by surrounding environmental flows (Ho et al., 2004). A direct cause that determines typhoon pathways is associated with the location of the WPSH. TC location induced by different synoptic environments can produce different remote rainfall characteristics. For this reason, the present study performs composite analyses for two different groups of TCs: TCs making landfall in China (LT cases) and TCs over the East China Sea (OT cases). Among 69 HR cases, 27 LT cases and 19 OT cases are selected (Table 1 and Fig. 4). Twenty-three cases of TCs landfalling over Taiwan or China 12 h after $T-0$ are excluded in the composite analysis. Twenty TCs among the LT cases dissipated after landfall, while six TCs approached the Korean peninsula with the strength of a TD or cyclone. Most TCs of OT cases showed northeastwardly paths when approaching Korea (four TCs) and Japan (nine TCs).

Remote TCs that can be related to HR over the Korean peninsula occur mainly in July, August, and September (Fig. 5a). The monthly number of LT events is evenly distributed for these three months, whereas OT events increase toward September. These frequency variations may be related to the location of the WPSH. On average, the WPSH retreats to the east in August and September as compared to June and July (Kim et al., 2008). TC strengths are generally weaker in LT cases than in OT cases, mainly because of rapid intensity decay with landfall (Fig. 5b, c). Figure 5d shows the duration of HR over the Korean peninsula after $T-0$. Rainfall continues for more than 72 h in LT cases, although the increase in rainfall rate decreases slightly after 48 h. However, for OT events in which TCs do not pass through or close to the Korean peninsula (EO events in Fig. 5d), HR does not continue as long as in LT events (EL). Increased rainfall for EO cases slows noticeably after 36 h.

4. Influence of remote TCs on HR over South Korea – composite analysis

Figure 6 shows composite maps of 850-hPa height, wind fields at 850 and 200 hPa, and vertical pressure velocity at 500 hPa for the HR and NR groups. Several important differences between the HR and NR composites can be found. At low levels, a strong ridge from the WPSH extends towards mid-eastern China in the NR composite (Fig. 6c), whereas the ridge over mid-eastern China is almost cut-off from the WPSH in the HR composite (Fig. 6a). As a result, in the HR composite, a belt of strong moisture transport extends to the Korean peninsula along the northwestern flank of the WPSH with a significant column-integrated moisture flux convergence (CIMFC) (Banacos and Schultz, 2005; van Zomeren and van Delden, 2007) over the peninsula (Fig. 6a). Conversely, moisture transport toward the peninsula is blocked by the ridge in the NR composite (Fig. 6c). The timing and strength of the upstream trough seem to be a key in the extension of the strong ridge from the WPSH towards mid-eastern China (Fig. 6a, c).

Important differences can also be found at upper levels (Fig. 6b, d). In the HR composite, a well-defined upper-level jet streak (ULJS) is found over the northern Korean

Table 1. Heavy rainfall events considered for the present composite analysis

TC (Number ID)	Initiation (UTC)	P (hPa)	D (km)	6 h rainfall	Max. station	24 h rainfall	Max. station
LT – 27 cases							
ELLEN (8309)	00 UTC 9 September	965	1806	64.5	Seongsanpo	118.5	Seongsanpo
WYNNE (8402)	12 UTC 25 June	985	2441	58.1	Yeongju	143.1	Geoje
JUNE (8412)[a]	18 UTC 30 August	985	1792	71.5	Jeongeup	174.5	Ganghwa
TESS (8516)	06 UTC 6 September	980	2219	77.0	Incheon	84.6	Gumi
PEGGY (8607)	00 UTC 11 July	975	1925	118.1	Boryeong	130.5	Boryeong
NONAME (8609)	00 UTC 21 July	996	2434	46.8	Gumi	51.0	Gumi
WARREN (8806)	12 UTC 19 July	980	1989	90.7	Hongcheon	284.5	Jecheon
SARAH (8919)	00 UTC 14 September	1004	1208	60.6	Boryeong	181.1	Boryeong
NATHAN (9004)	12 UTC 18 June	994	2450	171.0	Ganghwa	197.0	Ganghwa
OFELIA (9005)[a]	18 UTC 23 June	985	1382	86.6	Seoul	161.0	Hongcheon
YANCY (9012)	00 UTC 20 August	980	1077	60.5	Seogwipo	162.1	Sancheong
DOT (9017)	18 UTC 8 September	992	1816	79.8	Icheon	158.0	Chungju
AMY (9107)	18 UTC 19 July	985	1950	74.0	Jecheon	138.0	Jecheon
KORYN (9302)	18 UTC 27 June	975	2149	45.5	Jeongeup	134.0	Jeongeup
SALLY (9616)	18 UTC 8 September	940	2080	46.0	Suncheon	51.5	Suncheon
VICTOR (9712)	00 UTC 3 August	992	1915	73.6	Yeongwol	390.0	Ganghwa
TODD (9806)	06 UTC 20 September	1002	685	80.7	Seogwipo	142.3	Seogwipo
WENDY (9914)[a]	00 UTC 5 September	1006	1392	63.4	Tongyeong	121.2	Ulleungdo
CHANCHU (0010)[a]	18 UTC 23 August	996	1547	82.0	Boryeong	135.0	Boryeong
KAMMURI (0212)	12 UTC 5 August	992	1887	149.0	Inje	241.5	Inje
BILIS (0604)	00 UTC 15 July	990	1699	131.0	Gangneung	293.0	Hongcheon
KAEMI (0605)	12 UTC 25 July	990	1563	62.0	Imsil	164.0	Uiseong
PABUK (0706)[a]	18 UTC 11 August	994	1459	90.5	Heuksando	135.0	Jangheung
KROSA (0715)	06 UTC 07 October	985	1145	71.5	Namhae	94.5	Busan
KALMAEGI (0807)[a]	18 UTC 18 July	996	1305	150.0	Cheongju	197.0	Cheongju
FUNG-WONG (0808)	00 UTC 30 July	996	1416	67.5	Chuncheon	67.5	Chuncheon
NURI (0812)	06 UTC 22 August	980	1823	74.5	Haenam	94.0	Sokcho
OT – 19 cases							
AGNES (8118)[a]	18 UTC 28 August	975	1474	105.5	Seongsanpo	171.0	Seongsanpo
MAC (8604)	18 UTC 28 May	1000	1061	51.7	Seogwipo	67.1	Namhae
VERNON (8706)	00 UTC 21 July	985	1654	150.5	Icheon	436.0	Buyeo
DINAH (8712)	12 UTC 27 August	920	1863	89.5	Jecheon	104.3	Jeonju
SARAH (8919)	06 UTC 8 September	975	1357	100.0	Jeju	122.5	Jeju
JANIS (9210)	00 UTC 7 August	940	1255	112.8	Seoul	170.5	Hongcheon
STEVE (9308)	12 UTC 12 August	1004	1412	82.0	Muan	121.3	Wando
RYAN (9514)	18 UTC 22 September	955	972	43.9	Jeju	114.5	Sokcho
YANNI (9809)[a]	18 UTC 28 September	980	1150	115.0	Muan	223.3	Seogwipo
NARI (0116)	00 UTC 9 September	980	1027	58.5	Yeongcheon	273.5	Yeongdeok
NARI (0116)	18 UTC 13 September	975	871	79.0	Gwangju	97.0	Gwangju
NOGURI (0204)	12 UTC 10 June	985	785	57.5	Namwon	57.5	Namwon
KUJIRA (0302)	18 UTC 24 April	996	1082	43.0	Daejeon	130.0	Ulleungdo
LINFA (0304)	12 UTC 29 May	985	1309	97.5	Jindo	177.0	Jeju
ETAU (0310)	12 UTC 6 August	955	1591	156.5	Cheorwon	197.0	Cheorwon
CHOI-WAN (0315)	18 UTC 17 September	1000	1967	82.5	Ganghwa	211.0	Ganghwa
EWINIAR (0603)[a]	06 UTC 8 July	950	1213	42.5	Tongyeong	165.0	Masan
SHANSHAN (0613)	12 UTC 15 September	925	1182	50.5	Seongsanpo	52.0	Seongsanpo
NARI (0711)[a]	00 UTC 14 September	960	1050	75.5	Jeju	188.5	Goheung

Notes: The name of remote TCs with international ID number, HR initiation date and time (UTC), the central pressure of remote TCs (P), the distance between remote TC and 6-hourly maximum rainfall station (D), 6- and 24-hourly maximum rainfall amount (mm) and maximum observational stations. The superscript alphabet ([a]) refers to HR events in which TCs pass through or close to the Korean peninsula since T + 24.

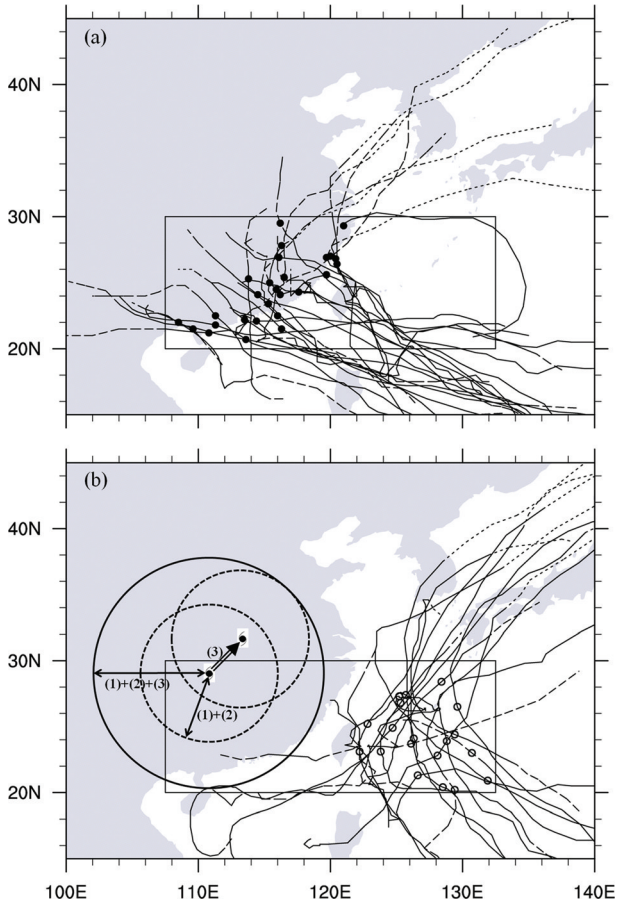

Fig. 4. Locations and tracks of remote TCs at T − 0 for: (a) landfalling TCs over China (LT cases, closed circles); and (b) TCs over the ocean (OT cases, open circles). The box region (20–30°N, 107.5–132.5°E) is the area of remote TC for composite analysis. The line types indicate cyclone grade: tropical storm and typhoon (solid line), TD (dashed line) and extratropical cyclone (dotted line). A schematic of the critical radius in this study is included in (b). The critical radius is calculated as the sum of: (1) the longest radius of (30 knots) winds provided by RSMC; (2) the maximum distance from the radius to the rain fields induced by the TC itself; and (3) the 6-houlry moving distance of TCs.

peninsula (Fig. 6b). The veering of winds from south–southwesterly at 850 hPa to west–southwesterly at 500 hPa (not shown) indicates that quasi-geostrophic (QG) forcing for ascent by warm-air advection is present over the peninsula. Significant large-scale upward motion is found over the Yellow Sea and the peninsula where a large amount of moisture is being transported by strong low-level southerlies, enhanced by a strong pressure gradient between the composite TC and the WPSH. Note that this rising motion is located on the right side of the ULJS entrance where a rising branch of secondary circulation can be found. The presence of both the ULJS and large-scale upward motion can provide a favorable situation for the development of deep and sustained heavy precipitation systems around the Korean peninsula. Further analysis concerning the vertical structure of atmospheric circulation associated with HR over the Korean peninsula will be provided later. In the NR composite, structures that can bring sustained HR are not found around the peninsula (Fig. 6d).

The HR cases were classified into two groups: TCs making landfall in China (LT) and TCs over the ocean (OT). Figure 7 shows composite maps of sea level pressure, wind fields at 1000 hPa, and CIMFC for LT and OT groups at different times (T − 24, T − 0, T + 24 and T + 48). At T − 24, a landfalling TC is found off the coast of southeastern China, producing a strong pressure gradient between the TC and the WPSH (Fig. 7a). As a result, strong southeasterlies blow along the eastern side of the TC, and significant moisture convergence occurs around the Shandong peninsula where the southeasterly meets the westerly to the north. At T − 0, TC strength has weakened slightly (Fig. 7b). However, the pressure gradient in the area between the TC and the WPSH remains

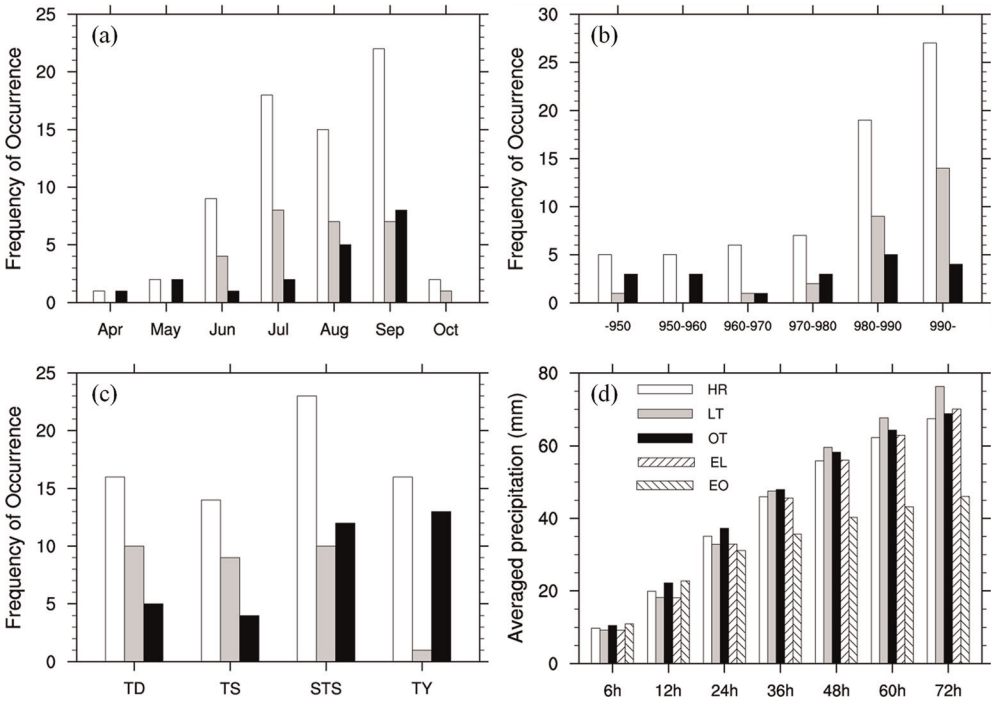

Fig. 5. Histogram of: (a) the monthly frequency; (b) minimum surface pressure; and (c) intensity category of remote TCs which are related to HR over the Korean peninsula. (d) Station-averaged precipitation for each time since T − 0 over the Korean peninsula. In each diagram, whole HR cases is represented by white bars, landfalling TC cases (LT) by grey bars, and oceanic TC cases (OT) by black bars. In (d), EL and EO are the same as LT and OT, respectively, except that TCs which approach the Korean peninsula are excluded. Intensity categories TD, TS, STS, and TY indicate tropical depression, tropical storm, severe tropical storm, and typhoon, respectively.

strong, and strong southerlies transport a large amount of moisture toward the Yellow Sea and the Korean peninsula where both significant CIMFC and pressure decreases are found. It can be seen that an extended trough develops from the TC centre to the Korean peninsula.

At T + 24, the pressure of the composite TC increases and the pressure gradient over the sea (to the west of the WPSH) is weakened significantly (Fig. 7c). TC dissipation at T + 24 may be exaggerated by the large variability in the location of landfalling TCs. However, the extended trough still remains well-defined, and significant CIMFC occurs over the Yellow Sea and southern half of the Korean peninsula, providing favorable conditions for possible HR over the peninsula. At T + 48, the extended trough remains, although it is weakened significantly (Fig. 7d). In addition, a larger CIMFC is found over the middle and northern part of the peninsula.

The composite map for the OT group shows a TC to the southeast of Taiwan at T − 24 (Fig. 7e). The weak strength of the composite TC may be due to the relatively large variability in the TC location. The axis of the ridge from the WPSH extends toward eastern China, passing through the Korean peninsula. At T − 0, the TC has moved northward to the east of Taiwan, and strong moisture transport toward the Korean peninsula is found over the northeastern part of the TC (Fig. 7f). Significant CIMFC is found over the southern half of the Korean peninsula and its neighbouring seas, providing favorable conditions for HR. As for the LT composite, a pressure decrease is found in the area of significant CIMFC (Fig. 7f, g). At T + 24, an extended trough develops from the TC centre to its northeast (Fig. 7g), the major area of CIMFC has moved to Japan, and the environment over the Korean peninsula becomes less favorable for sustained HR.

Large-scale flow patterns and moisture transport paths can show more clearly how remote TCs affect the environment for HR over the Korean peninsula. Synoptic-scale pressure patterns during remote TC events may be characterised by a major trough to the northwest, the WPSH to the southeast, and a TC to the south or southwest of the Korean peninsula (Fig. 8). We first look at LT composites. In LT composites, the pressure pattern allows two important forcings: (1) strong northward moisture transport over the sea between the TC and the WPSH; and (2) large-scale flow convergence between the westerlies associated with the trough to the northwest and southwesterlies along the northwest rim of the WPSH. These forcings can make significant CIMFC over the peninsula. At T − 48, the TC is over the sea to the

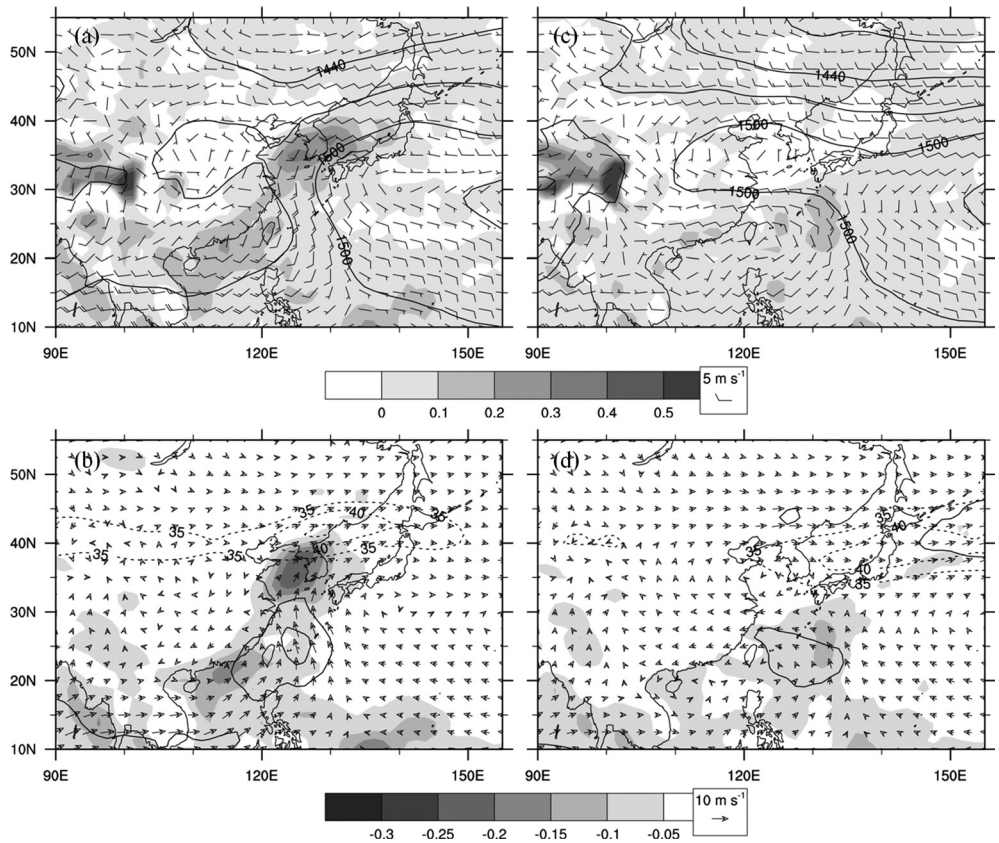

Fig. 6. Composite maps for T − 0 for 69 HR cases (left panels) and 103 NR cases (right panels): (a, c) wind fields (wind barb), geopotential height (every 30 m, solid lines) at 850 hPa, and CIMFC (every 0.1×10^{-4} from 0 g kg^{-1} s^{-1}, shaded); and (b, d) wind vectors at 850 hPa, isotachs for 200 hPa (every five from 35 m s^{-1}, dashed) and 850 hPa (every 2.5 from 10 m s^{-1}, solid lines), and vertical pressure velocity at 500 hPa (every −0.05 from −0.05 Pa s^{-1}, shaded).

southeast of Taiwan, and moisture is transported mainly to the northwest of the TC (Fig. 8a). A strong ridge is extended to eastern China from the WPSH, and large-scale flow convergence is found at the northwestern edge of this ridge, far inland to the northwest of the Shandong peninsula. At T − 24, the TC has moved northwestward, making landfall over the southeastern coast of China and moisture transport towards the Korean peninsula has become stronger (Fig. 8b). The ridge over eastern China has weakened and the zone of large-scale flow convergence is found near the Shandong peninsula. At T − 0, the TC has moved westward into southern China (Fig. 8c). Most of the moisture transport over the sea between the TC and the WPSH is directed toward the Korean peninsula with high equivalent potential temperature (θ_e) air moving over the peninsula. Furthermore, the zone of large-scale flow convergence has moved to the west coast of the Korean peninsula. At T + 24, the pressure of the composite TC has increased, changing into a weak trough in southern China. However, the two synoptic conditions (forcings) for HR over the Korean peninsula are maintained. TC dissipation at T + 24 may be exaggerated by the large variability in the location of landfalling TCs (Fig. 7c).

In composite maps for OT events, HR over the Korean peninsula occurs in a somewhat different manner from that of the LT composites. At T − 48, the composite TC for the OT group is not well-defined, mainly due to a relatively large variability in TC locations (Figs. 7e and 8e). The TC becomes better defined as it moves northward. At T − 24, the composite TC is located southeast of Taiwan (Fig. 8f), at which time the TC does not strongly affect the Korean peninsula very much. At T − 0, the composite TC has moved northward to the east of Taiwan (Fig. 8g). Moisture transport toward the Korean peninsula is due to the southerlies in the northeastern part of the TC. The southerlies have been enhanced by the presence of a quasi-stationary WPSH. At T + 24, the TC has moved close to Kyushu, Japan, and moisture transport is found mainly along the Japanese islands (Fig. 8h). The synoptic environment over the peninsula is no longer favorable for sustained HR, unlike the LT composite. As the TC moves northward,

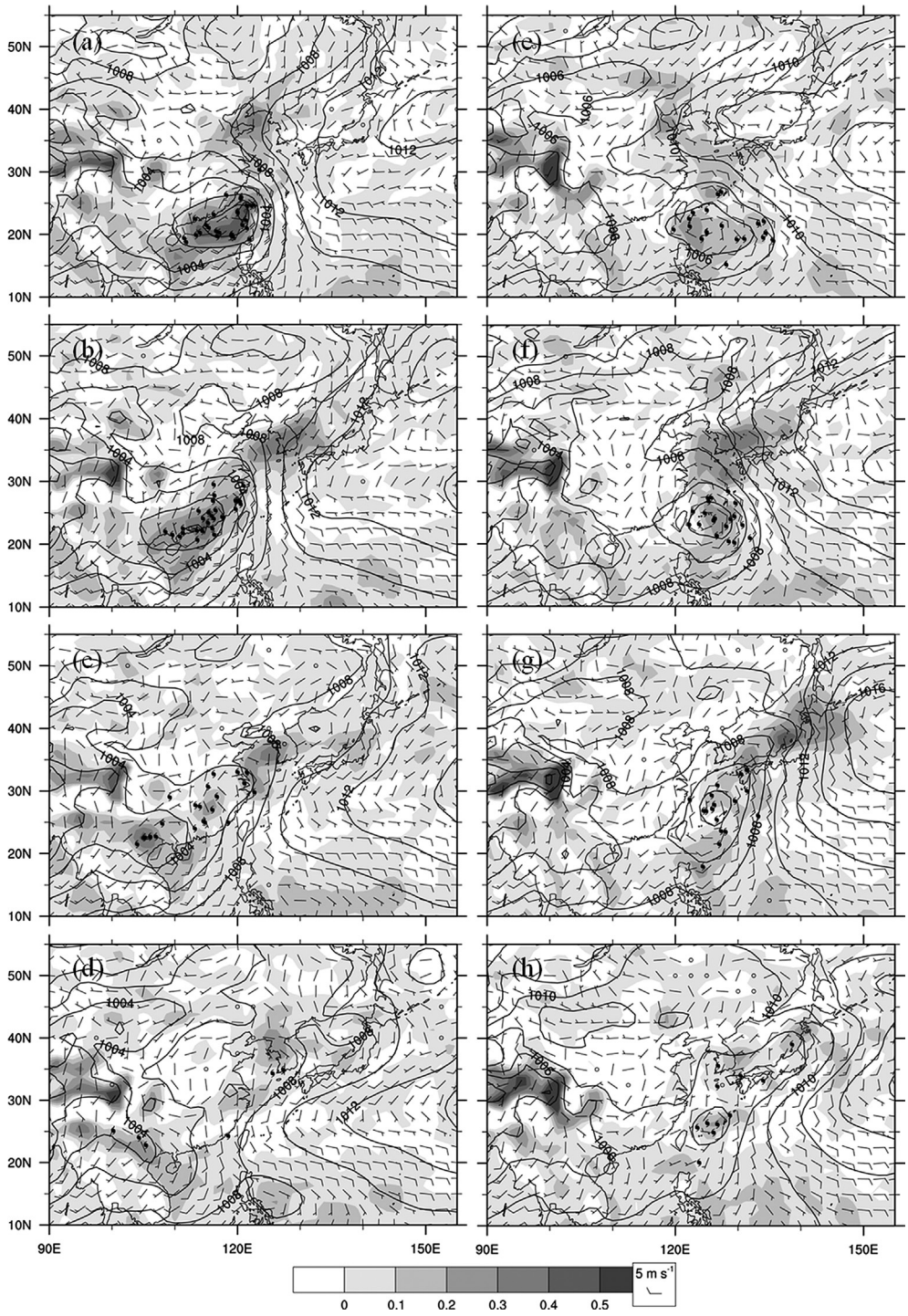

Fig. 7. Composite map of sea level pressure (every 2 hPa, solid lines), wind fields at 1000 hPa (wind barb), column-integrated MFC (every 0.1×10^{-4} from 0 g kg^{-1} s^{-1}, shaded) for LT composite (left panels) and OT composite (right panels) at: (a, e) T − 24; (b, f) T − 0; (c, g) T + 24; and (d, h) T + 48. TC symbols indicate TC locations.

the WPSH retreats eastward. At the same time, θ_e ridge and the zone of large-scale flow convergence move eastward.

The relationship between the upper- and low-level jets (LLJs) is examined. Figure 9 shows a composite of wind vectors at 850 hPa, isotachs for 850 and 200 hPa levels and vertical pressure velocity at 500 hPa for LT and OT events. At T − 48 for the LT composite, a weak ULJS is found at 40°N, 90–105°E. A rising motion found

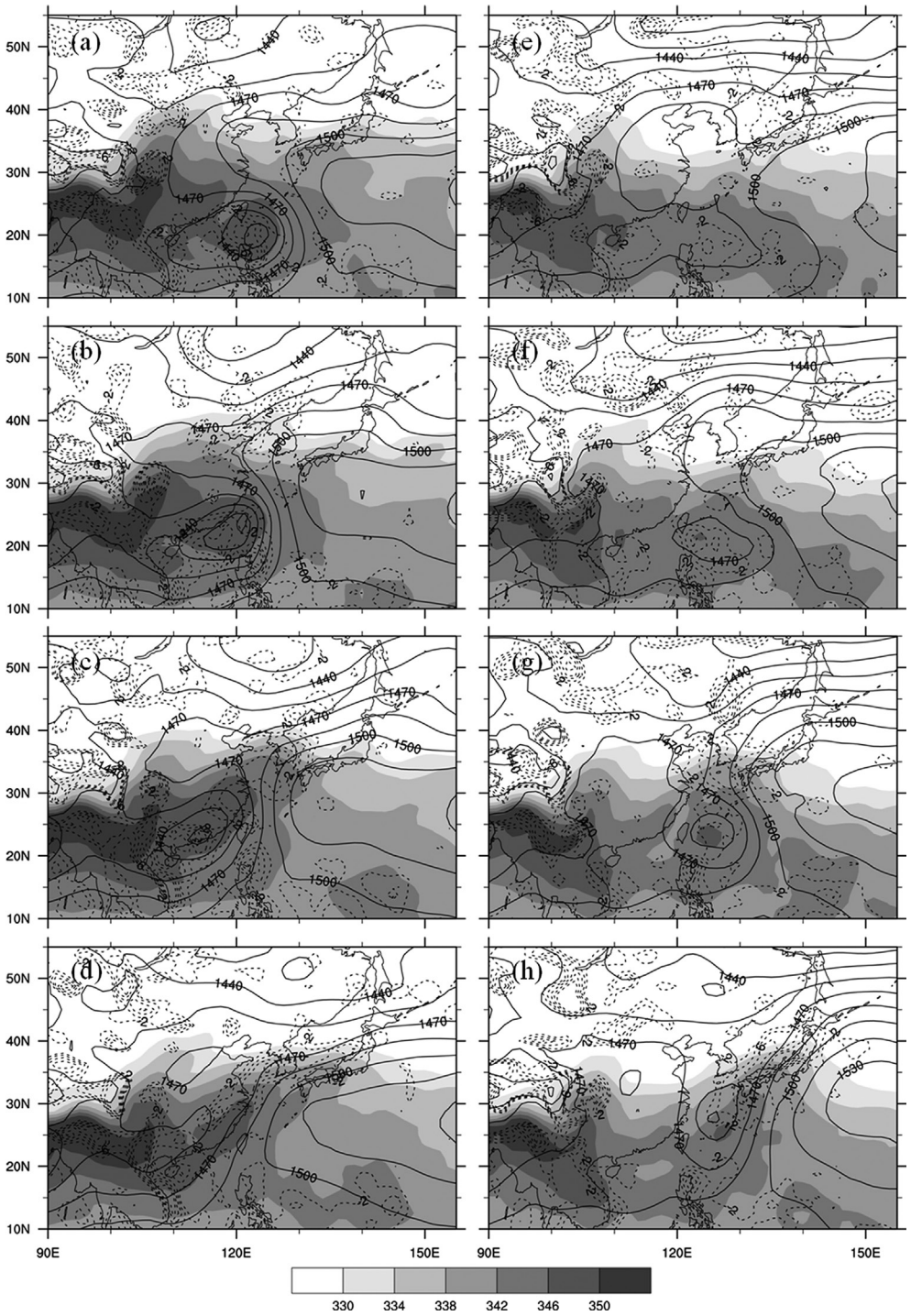

Fig. 8. Composite of geopotential height (every 15 m, solid), equivalent potential temperature (every 4 K, shaded), and horizontal divergence (every 2×10^{-6} s^{-1} from -2×10^{-6} s^{-1} to -10×10^{-6} s^{-1}, dashed) at 850 hPa for LT (left panels) and OT (right panels) at: (a, e) T − 48; (b, f) T − 24; (c, g) T − 0; and (d, h) T + 24.

to the east (Fig. 9a) is due to the large-scale convergence of air flow associated with the trough to the north and southerlies to the south. The composite TC is located over the sea to the southeast of Taiwan. The ULJ extends to the east of northern Korea at T − 24, and the area of rising motion has moved to the Shandong peninsula (Fig. 9b). At T − 0, when HR begins, the area of rising motion has moved over the Yellow Sea, covering the

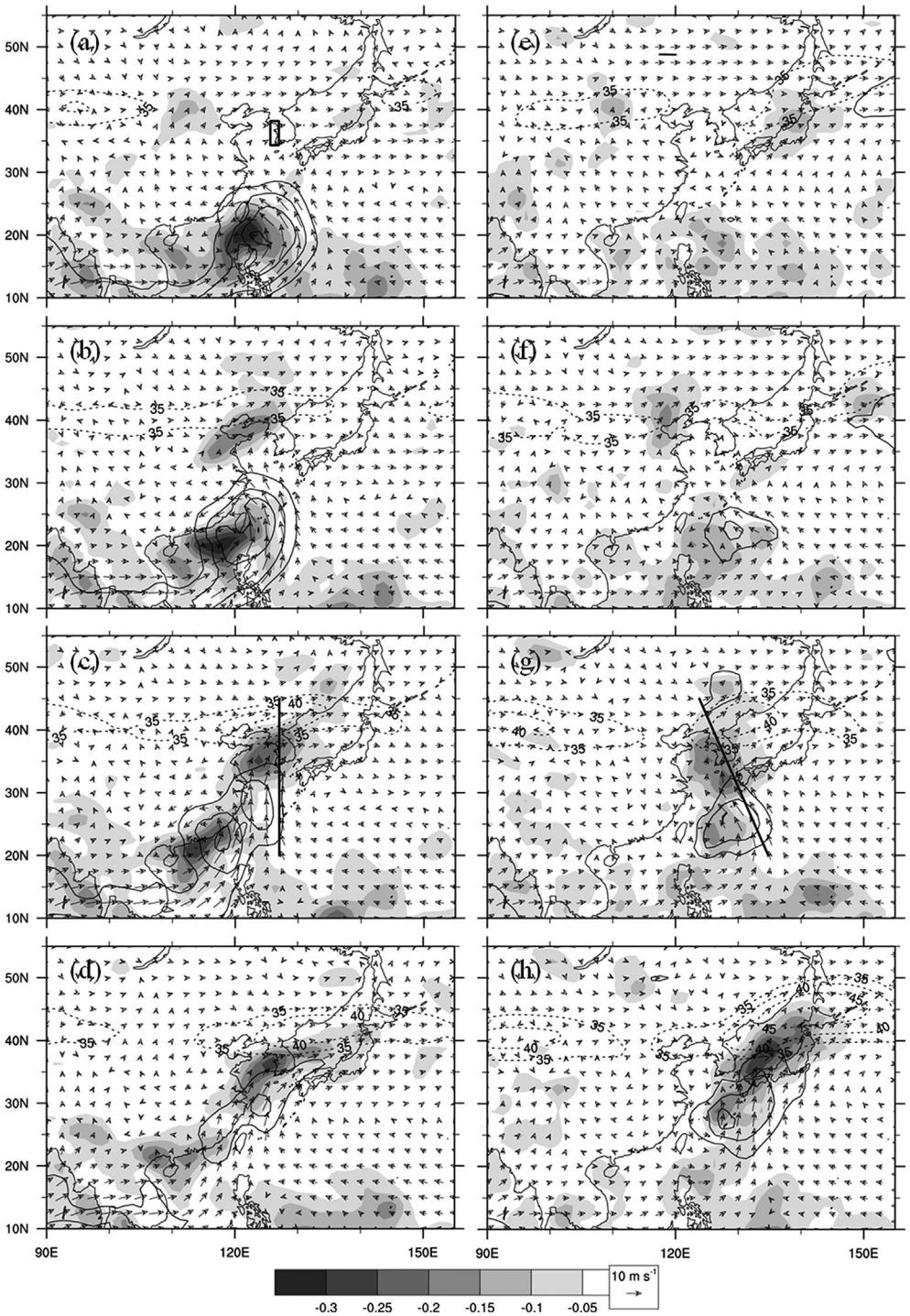

Fig. 9. Composite of wind vectors at 850 hPa, isotachs for 200 hPa (every five from 35 m s^{-1}, dashed lines), 850 hPa (every 2.5 from 10 m s^{-1}, solid lines) and vertical pressure velocity at 500 hPa (every -0.05 from -0.05 Pa s^{-1}, shaded) for LT (left panels) and OT (right panels) at: (a, e) T − 48; (b, f) T − 24; (c, g) T − 0; and (d, h) T + 24.

whole Yellow Sea and the Korean peninsula and the strength of the rising motion has increased significantly. A well-defined ULJS has developed over the northern Korean peninsula with a maximum speed greater than 45 m s^{-1}. Its entrance is located to the northwest of the maximum rising motion. At this hour, the west coast of the Korean peninsula is under strong rising motion and is also experiencing strong large-scale convergence of

westerlies to the north and a south–southwesterly LLJ to the south. Both large and mesoscale (enhanced LLJ) forcings are present over the Korean peninsula. At T + 24, the belt of strong moisture transport is maintained, even though the winds over the sea around Taiwan have weakened significantly (Fig. 9d).

Figures 9 and 10 show that the ULJS and its secondary circulation are coupled with the vertical circulation associated with the large-scale flow convergence ahead of strong low-level southerlies (Fig. 9c, d and 10a). The strongest rising motion is located to the right side of the ULJS entrance, and a region of convective instability is found below this rising motion (Fig. 10a). The convective instability is enhanced by the strong transport of warm and moist air from the south. These phenomena provide an environment that is quite favorable for mesoscale convection over the Korean peninsula.

In the OT composites, the weak ULJS at 40°N and the location of the rising motion at T − 48 and T − 24 are similar to those for LT composites (Fig. 9e, f). Winds associated with the composite TCs are much weaker than those with the LT composites. At T − 0, when strong southerlies in the northern part of the composite TC directly affect the south coast of the Korean peninsula, rising motion occurs in a wide area over the northern part of the TC, including the whole Korean peninsula

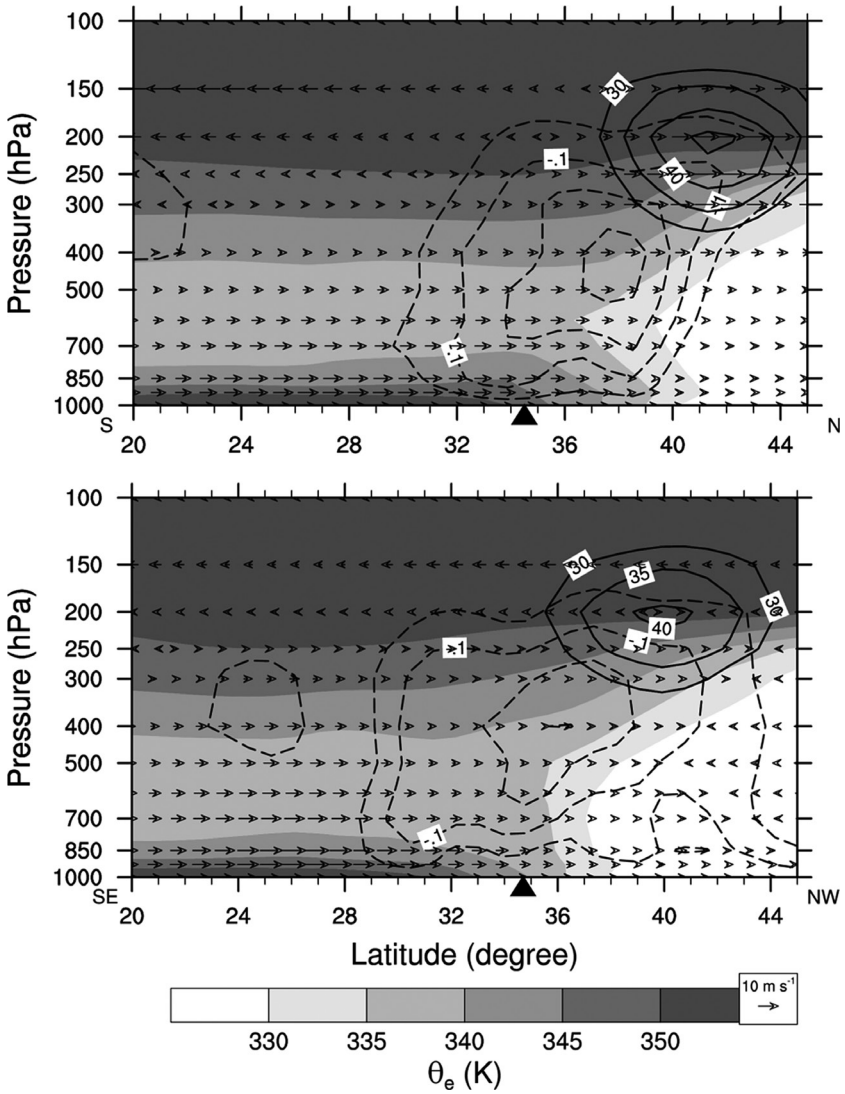

Fig. 10. Vertical cross sections of equivalent potential temperature (every 5 K, shaded), vertical pressure velocity (every −0.05 from −0.05 Pa s^{-1}, dashed lines), the total wind speed (every five from 30 m s^{-1}, solid lines), and horizontal flow in the plane of the cross section (arrows in m s^{-1}) at T − 0 for: (a) LT composite; and (b) OT composite. Each cross-section orientation is marked in Fig. 9c, g, respectively. Triangles indicate the location of the southern coast line of the Korean peninsula.

(Figs. 9g and 10b). In addition, a direct coupling of the ULJS and low-level southerlies associated with the TC can be found. However, the system moves eastward relatively quickly, leaving the Korean peninsula after 24 h with relatively short periods of HR over the peninsula (Fig. 9h). A similar remark was made in Section 3 concerning the duration of HRs related to TCs in the EO cases (Fig. 5d).

The rising motion over the Korean peninsula (in Figs. 9 and 10) is due to several forcings: large-scale convergence, warm advection, and convective heating. The cross sections in Fig. 10 clearly show the influence of low-level winds associated with the composite TCs: low-level transport of warm and moist air toward the Korean peninsula, convergence of low-level winds and significant large-scale rising motion, and convective instability in the lower troposphere over the peninsula and the sea to its south. Temporal variation of the environment along the west coast of southern Korea can be seen in Fig. 11 in terms of the equivalent potential temperature difference between 500 and 850 hPa (θ_{e500}–θ_{e850}) and the CIMFC. The values are the average over the grids in the box shown in Fig. 9a. For both LT and OT composites, CIMFC tends to increase with time until T − 0 (Fig. 11). After T − 0, it maintains significant magnitude for the LT composite, whereas it tends to decrease with time for the OT composite. The difference in the duration of the HR between LT and OT cases has the same tendency as that in CIMFC. The difference (θ_{e500}–θ_{e850}) shows approximately the opposite temporal tendency, rapidly decreasing between T − 12 and T − 0 and further decreasing until T + 12. After T + 12, a continuous increase is found. The destabilisation around T − 0 is driven primarily by increases in low-level equivalent potential temperature. Based on these results, the influence of the composite TC can be summarised as an increase of convective instability in the lower troposphere towards T − 0 and a decrease afterwards.

Figure 12a, c show that the warm advection by southerly and southeasterly winds occurred over the Korean peninsula at T − 0 for LT and OT composite, respectively. Therefore, the convergence of Q vector (Bluestein, 1992) at 700 hPa in Fig. 12 indicates that the QG forcing for ascent by warm advection agrees with the vertical motion over the western area of the Korean peninsula in Fig. 9. This result shows that warm advection is an important physical mechanism in driving vertical motion over the area. The QG forcing for ascent is also in agreement with the LLJ moisture transport maximum (Fig. 7). While warm advection over the Korean peninsula weakened, the convergence of Q vector over the Yellow Sea was maintained until T + 24 in the LT composite (Fig. 12b), the area of maximum warm advection and the Q vector convergence moved eastward into Japan in the OT composite (Fig. 12d).

Within this favorable synoptic-scale environment, mesoscale features can act as focusing mechanisms for vigourous ascent (Galarneau et al., 2010). Fig. 13 shows the composite of geopotential height, equivalent potential temperature (θ_e) and Petterssen frontogenesis (Keyser et al., 1986; Bluestein, 1993) at 925 hPa for LT and OT. The maximum of frontogenesis coincides with the equivalent potential temperature (θ_e) ridge on the northwestern edge of WPSH at 925 hPa (Fig. 13a, c). Warm and moist air between composite TC and WPSH is transported to the confluent region by southerly or southeasterly winds along the edge of WPSH. As the composite TC was landfalling

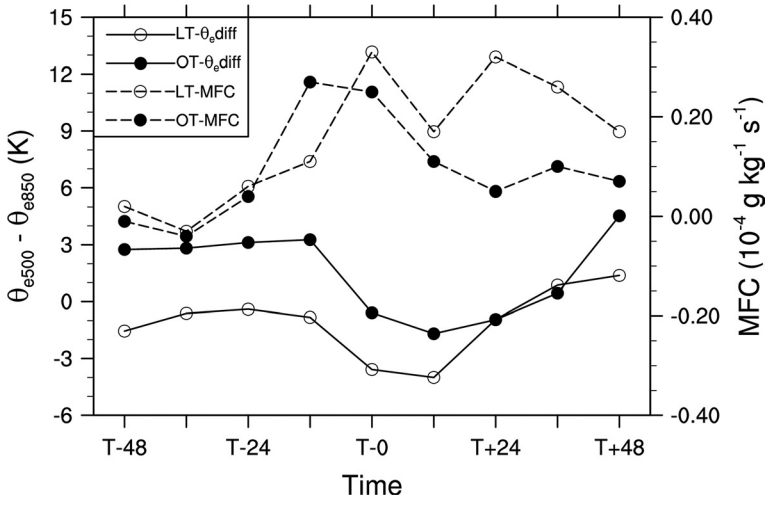

Fig. 11. Time series of the equivalent potential temperature difference between 500 and 850 hPa ($\theta_e$diff = θ_{e500}–θ_{e850}, solid lines) and CIMFC (dashed lines) for LT (open circle) and OT (blackened circle). These values are the average over grids in the box shown in Fig. 9a.

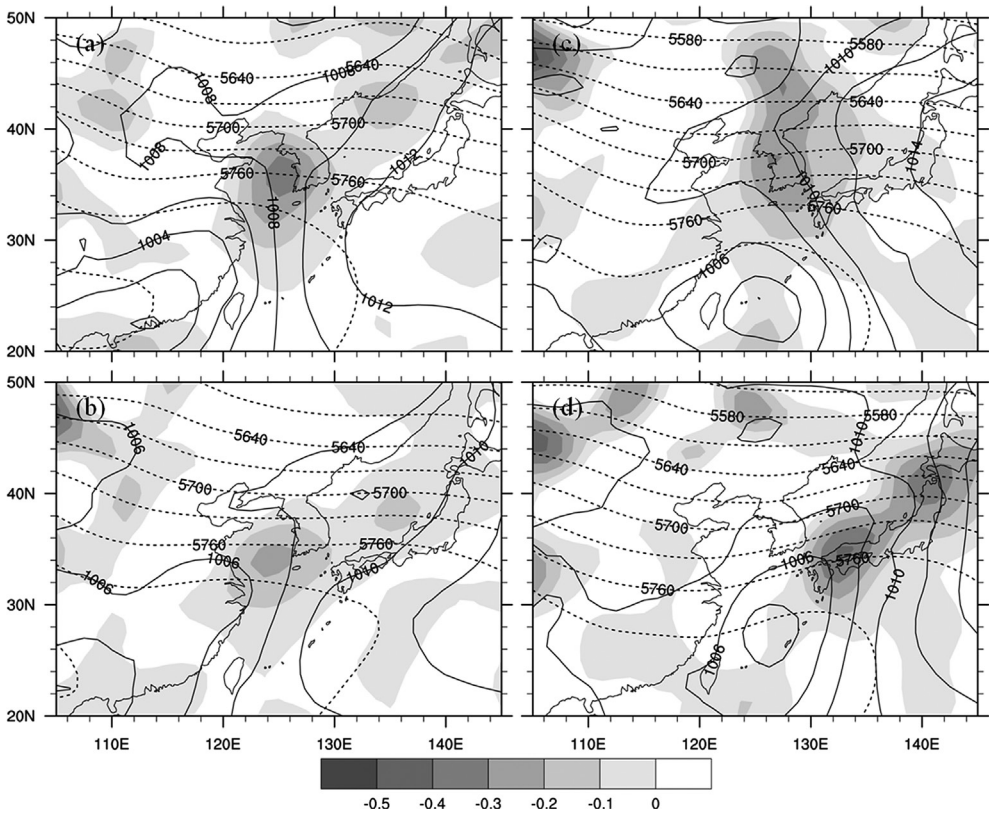

Fig. 12. Composite of sea level pressure (every 2 hPa, solid lines), 1000–500 hPa thickness (every 30 m, dashed lines), and divergence of Q-vector (every 0.1×10^{-12} Pa m^{-2} s^{-1}, shaded) at 700 hPa for LT (left panels) and OT (right panels) at: (a, c) T − 0; and (b, d) T + 24.

over China, the maximum of frontogenesis over the peninsula was maintained until T + 24 in the LT composite (Fig. 13b). The low-level frontogenetical forcing is also in agreement with the vertical motion over the western area of the Korean peninsula in Fig. 9. The low-level frontogenetical forcing along a baroclinic zone can act as a focusing mechanism for strong rising motion. On the other hand, composite TC moved northward, and WPSH retreated toward the east of western Pacific for the OT composite at T + 24 (Fig. 13d). The maximum of frontogenesis and the θ_e ridge migrated eastward faster. These findings show that low-level frontogenesis acts as possible mesoscale mechanism for producing HR over the peninsula. However, additional mesoscale features such as topographic barriers, convective heating can be examined through case studies.

Figure 14 shows conceptual models of the synoptic-scale environment associated with HR over the Korean peninsula occurring with remote TCs for LT and OT at T − 24, T − 0, and T + 24. Large-scale flow patterns can show more clearly how remote TCs affect the environment for HR over the Korean peninsula. At T − 0, synoptic-scale pressure patterns during remote TC events may be characterised by a major trough to the northwest, the WPSH to the southeast, and a TC to the south or southwest of the Korean peninsula (Figs. 8 and 14b, e).

In the LT composite, a landfalling TC is found off the coast of southeastern China, producing a strong pressure gradient between the TC and the WPSH at T − 24 (Fig. 14a). As a result, strong southeasterlies blow along the eastern side of the TC, and significant moisture convergence occurs around the Shandong peninsula where the southeasterly meets the westerly to the north. The ULJ extends to the northern Korean peninsula at T-24, and the area of rising motion has moved to the Shandong peninsula. At T − 0 (Fig. 14b), TC strength has weakened slightly. However, the pressure gradient in the area between the TC and the WPSH remains strong, and strong southerlies transport a large amount of moisture toward the Yellow Sea and the Korean peninsula where pressure decreases are found. It can be seen that an extended trough develops from the TC centre to the Korean peninsula. The composite TC has moved westward into southern China. Most of moisture transport over the sea between the TC and the WPSH by LLJ is directed toward the Korean peninsula with high-θ_e air moving over the peninsula. Furthermore, the zone of large-scale flow convergence of westerlies to the north and a south–southwesterly LLJ to the south has moved to the west coast of the Korean

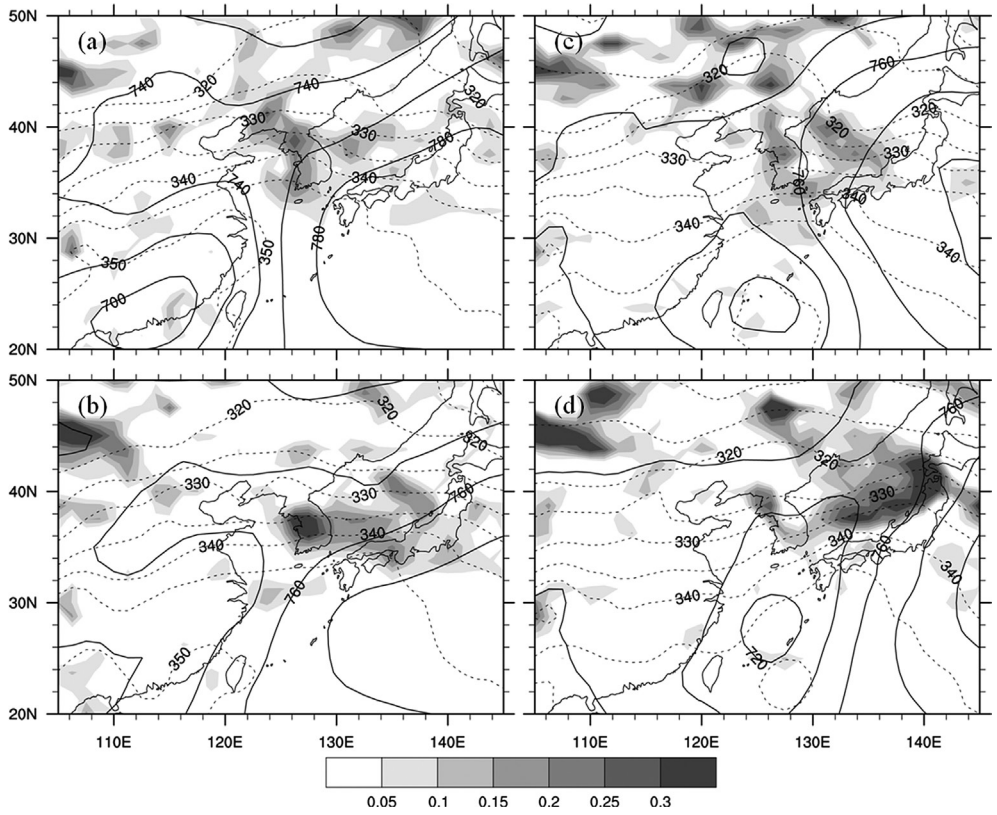

Fig. 13. Composite of geopotential height (every 20 m, solid), equivalent potential temperature (every 5 K, dashed), and Petterssen frontogenesis (every 0.05 K $[100\,\mathrm{km}]^{-1}\,[3\,\mathrm{h}]^{-1}$, shaded] at 925 hPa for LT (left panels) and OT (right panels) at: (a, c) T − 0; and (c, d) T + 24.

peninsula. The area of rising motion has moved over the Yellow Sea, covering both the whole Yellow Sea and the Korean peninsula, and the strength of the rising motion has increased significantly. The ULJS and its secondary circulation are coupled with the vertical circulation associated with the large-scale flow convergence ahead of strong low-level southerlies. At T + 24 (Fig. 14c), the pressure of the composite TC increases, and the pressure gradient over the sea (to the west of the WPSH) is also weakened significantly. However, the extended trough still remains well-defined, and significant LLJ occurs over the Yellow Sea and the southern half of the Korean peninsula. This pattern can provide favorable conditions for HR over the peninsula. The belt of strong moisture transport is maintained, even though the winds over the sea around Taiwan have weakened significantly. It can be seen that the ULJS and its secondary circulation are coupled with the vertical circulation associated with the large-scale flow convergence ahead of strong low-level southerlies.

In OT composites, the composite TC is located southeast of Taiwan at T − 24 (Fig. 14d), at which time the TC does not affect the Korean peninsula considerably. The axis of the ridge from the WPSH extends toward eastern China, thereby passing through the Korean peninsula. Winds associated with the composite TCs are much weaker than those with the LT composites. At T − 0 (Fig. 14e), the TC has moved northward to the east of Taiwan, and the LLJ toward the Korean peninsula is found over the northeastern part of the TC. Moisture transport toward the Korean peninsula is due to the southerlies in the northeastern part of the TC. The southerlies have been enhanced by the presence of a quasi-stationary WPSH. When strong southerlies in the northern part of the composite TC directly affect the south coast of the Korean peninsula, rising motion occurs in a wide area over the northern part of the TC, including the whole Korean peninsula. Furthermore, a direct coupling of the ULJS and low-level southerlies associated with the TC can be found. At T + 24 (Fig. 14f), the TC has moved close to Kyushu, Japan and moisture transport is found mainly along the Japanese islands. As the TC moves northward, the WPSH retreats eastward. At the same time, θ_e ridge and the zone of large-scale flow convergence move eastward. An extended trough develops from the TC centre to its northeast, the major area of CIMFC has moved to Japan, and the environment over

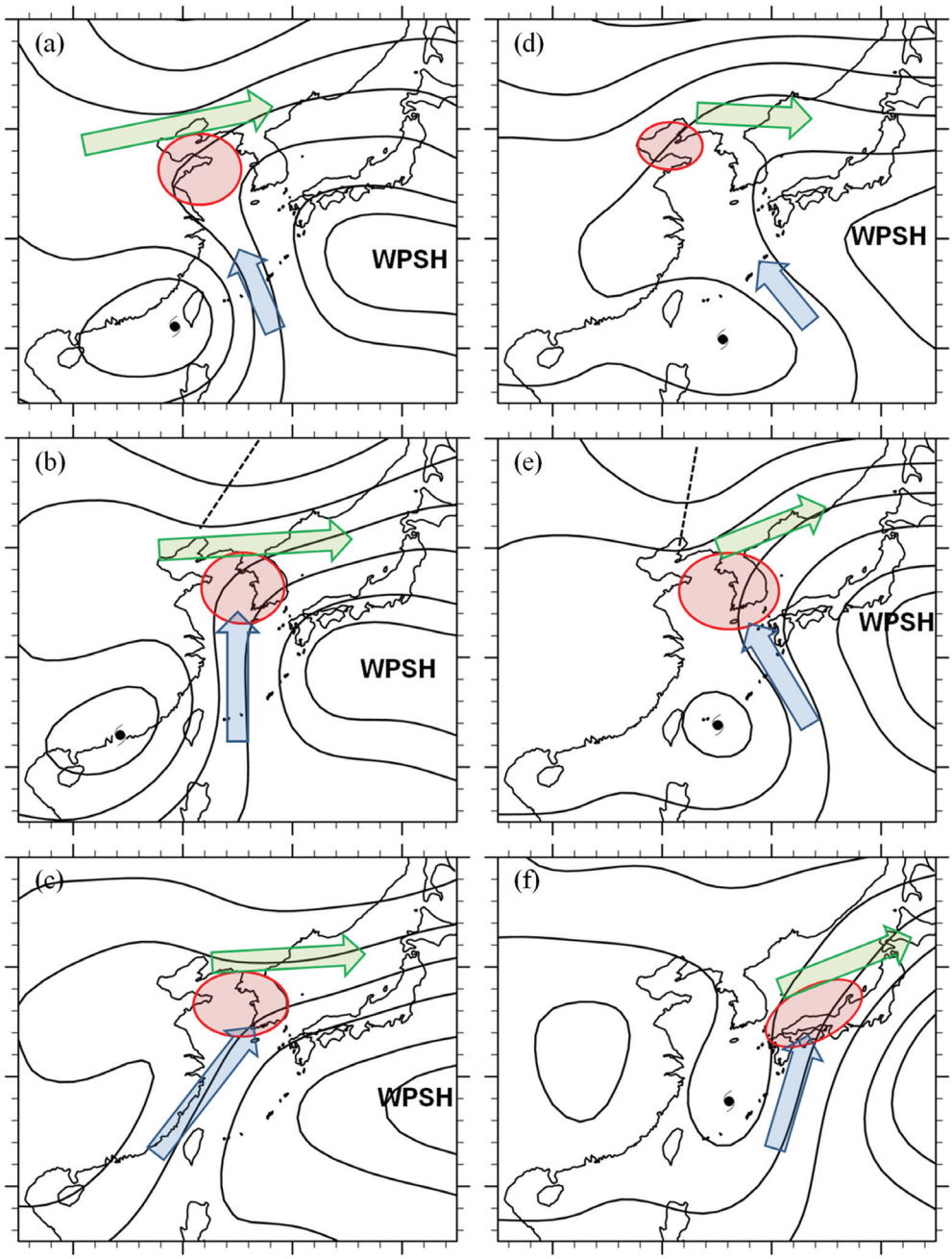

Fig. 14. Conceptual models of synoptic-scale environment associated with HR over the Korean peninsula occurring with remote TCs for LT (left panels) and OT (right panels) at: (a, d) T − 24; (b, e) T − 0; and (c, f) T + 24. The symbols indicate smoothed 850 hPa geopotential height (black line), LLJ (blue arrow), ULJ (green arrow), low-level convergence and high-CIMFC (red area), and synoptic-scale trough (dashed line).

the Korean peninsula becomes less favorable for sustained HR. The synoptic environment over the peninsula is no longer favorable for sustained HR, unlike the LT composite. The system moves eastward relatively quickly, leaving the Korean peninsula after 24 h with relatively short periods of HR over the peninsula.

5. Summary and conclusions

The remote effects of TCs on HR over the Korean peninsula were investigated through statistical and composite analyses for the 29-year period 1981–2009. This study used the observed precipitation data from manned stations

of the KMA, TC best-track data archived by the RSMC, and JRA-25 data.

According to statistical analysis, the 29-year mean annual amount of rainfall occurring with TCs within a 3000 km distance is 658 mm, accounting for 49% of the 29-year mean total rainfall amount of 1340 mm. About 32% of the mean annual total amount occurs with TCs in the distance range of 1200–2800 km. These results show that remote TCs are an important element of a favorable environment for HR around the Korean peninsula during summer. Statistical analysis has revealed that the probability of HR over the Korean peninsula is higher with TCs landfalling in southern and eastern China than in other areas (10–20% of TCs along the coast and 14–36% of TCs on the inland of southern China). These results agree with case studies which explain the effects of TCs in southern China as a factor favoring HR over the Korean peninsula. In addition, more than 10% of TCs over Taiwan and the southern East China Sea are also accompanied by HR over the peninsula. Based on these results, composite analysis has been carried out for those cases where TCs lie within the box area (20–30°N, 107.5–132.5°E).

To examine the typical environments associated with HR over the peninsula related to remote TCs, composites are constructed for HR and NR. In the HR composite, the synoptic-scale pressure pattern during remote TC events is characterised by a synoptic-scale trough to the northwest, the WPSH to the southeast and a TC to the southwest of the Korean peninsula. A belt of strong moisture transport extends to the Korean peninsula along the northwestern flank of the WPSH. Significant large-scale upward motion is found over the Yellow Sea and the peninsula where a large amount of moisture is being transported by strong low-level southerlies, which is enhanced by an increased pressure gradient between the composite TC and the WPSH. The rising motion is located in the right side of the ULJS entrance where a rising branch of secondary circulation can be found. The presence of ULJS and large-scale upward motion can provide a favorable situation for the development of deep and sustained heavy precipitation systems around the Korean peninsula. On the other hand, moisture transport toward the peninsula is blocked by the ridge extending from the WPSH in the NR composite, and structures that can bring sustained HR are not found around the peninsula.

The HR cases were classified into two groups: TCs making landfall in China (LT) and TCs over the southern East China Sea (OT). In the LT composite, the pressure pattern allows two important forcings at $T - 0$: (1) strong northward moisture transport over the sea between the TC and the WPSH; and (2) large-scale flow convergence between the westerlies associated with the trough to the northwest and the southwesterlies along the northwest rim of the WPSH. At $T + 24$, the pressure of the composite TC increases and the pressure gradient over the sea (to the west of the WPSH) also weakens significantly. However, the extended trough still remains well-defined, and significant CIMFC occurs over the Yellow Sea and the southern half of the Korean peninsula. This pattern can provide favorable conditions for HR over the peninsula.

In the OT composite, the composite TC has moved northward to the east of Taiwan, and strong moisture transport toward the Korean peninsula is found over the northeastern part of the TC at $T - 0$. Significant CIMFC is found over the southern half of the Korean peninsula and its neighbouring seas, providing favorable conditions for HR. As for the LT composite, a pressure decrease is found in the area of significant CIMFC, and an extended trough develops at $T + 24$ from the TC centre to its northeast. At $T + 24$, the area of major CIMFC has moved to Japan, and the environment over the Korean peninsula has become less favorable for sustained HR, unlike the LT composite. As the TC moves northward, the WPSH retreats eastward. At the same time, the θ_e ridge and the zone of large-scale flow convergence move eastward.

In both the LT and OT composites, the ULJS and its secondary circulation are coupled with the vertical circulation associated with large-scale flow convergence ahead of strong low-level southerlies. A strong rising motion is located to the right side of the ULJS entrance, and a region of convective instability and QG forcing for ascent by warm-air advection is found below this rising motion. The convective instability is enhanced by the strong transport of warm and moist air from the south. These conditions provide an environment that is favorable for mesoscale convection over the Korean peninsula.

The conceptual models summarise that remote TCs can affect HR over the Korean peninsula through active contribution to establishing convectively unstable environments and the large-scale convergence of air. Furthermore, this study shows that low-level frontogenesis acts as possible mesoscale mechanism for HR over the peninsula. Despite the differences in coordinates shifting and the regions, the composite results have notable similarities with the relevant physical mechanisms that result in PREs as presented in Galarneau et al. (2010) and Schumacher et al. (2011). However, additional mesoscale features such as topographic barriers, convective heating can be examined through case studies. This study has been focused on the environment and relationships based on synoptic-scale composite analysis. More specific relationship between HR over the Korean peninsula and remote TCs can be obtained through case studies with in-depth analysis.

According to these results, the long-lasting HR of LT cases and subsequent HR from TC's approaching the Korean peninsula after a remote rainfall event associated

with the TC in HR cases are critical for forecasters. Statistical analysis in this study can provide climatological guidelines for forecasters to anticipate the probability of HR over the Korean peninsula when TCs are in a remote area at some distance away from the Korean peninsula.

6. Acknowledgements

This work was funded by the KMA Research and Development Programme under Grant CATER 2006–2304. The reanalysis data for this study are from the Research Data Archive (RDA) which is maintained by the Computational and Information Systems Laboratory (CISL) at the National Center for Atmospheric Research (NCAR). The original data are available from the RDA (http://dss.ucar.edu) in dataset number ds625.0. The authors thank Professor. Yuqing Wang (University of Hawaii at Manoa), Professor. H. Joe Kwon (Kongju National University), Professor. Song-You Hong, and Professor. Hyun Mee Kim (Yonsei University) for helpful discussions and suggestions. Dr. Harald Lejenäs and two anonymous reviewers provided valuable comments and suggestions during the review process.

References

American Meteorological Society, (AMS). 2007. Hurricane forecasting in the United States: an Information Statement of the American Meteorological Society. *Bull. Amer. Meteor. Soc.* **88**, 950–953.

Atallah, E., Bosart, L. F. and Aiyyer, A. R. 2007. Precipitation distribution associated with landfalling tropical cyclones over the eastern United States. *Mon. Wea. Rev.* **135**, 2185–2206.

Banacos, P. C. and Schultz, D. M. 2005. The use of moisture flux convergence in forecasting convective initiation: historical and operational perspectives. *Wea. Forecasting*. **20**, 351–366.

Bluestein, H. B. 1992. *Synoptic-dynamic meteorology in midlatitudes*. Vol. I: principles of kinematics and dynamics. Oxford University Press, New York, 431 pp.

Bluestein, H. B. 1993. *Synoptic-dynamic meteorology in midlatitudes. Vol. II observations and theory of weather systems*. Oxford University Press, New York, 594 pp.

Bosart, L. F. and Carr, F. H. 1978. A case study of excessive rainfall centered around Wellsville, New York, 20–21 June 1972. *Mon. Wea. Rev.* **106**, 348–362.

Camargo, S. J. and Sobel, A. H. 2004. Formation of tropical storms in an atmospheric general circulation model. *Tellus*. **56A**, 56–67.

Chen, L.-S., Murata, A., Duan, Y., Chau, D. L., Li, Y., Black, P., Cheng, M. 2006. Observations and forecasts of rainfall distribution. Topic 0.3, Workshop Topic Reports of the Sixth WMO International Workshop on Tropical Cyclones (IWTC-VI), TMRP 72, WMO, 36–42.

Corbosiero, K. L., Dickinson, M. J. and Bosart, L. F. 2009. The contribution of eastern North Pacific tropical cyclones to the rainfall climatology of the southwest United States. *Mon. Wea. Rev.* **137**, 2415–2435.

Cote, M. R. 2007. *Predecessor rain events in advance of tropical cyclones*. M.S. thesis, Department of Atmospheric and Environmental Sciences, University at Albany, State University of New York, 200 pp.

Farfán, L. M. and Fogel, I. 2007. Influence of tropical cyclones on humidity patterns over southern Baja California, Mexico. *Mon. Wea. Rev.* **135**, 1208–1224.

Frank, W. M. 1977. The structure and energetics of the tropical cyclone I. Storm structure. *Mon. Wea. Rev.* **105**, 1119–1135.

Galarneau, T. J., Bosart, L. F. and Schumacher, R. S. 2010. Predecessor rain events ahead of tropical cyclones. *Mon. Wea. Rev.* **138**, 3272–3297.

Hanley, D., Molinari, J. and Keyser, D. 2001. A composite study of the interactions between tropical cyclones and upper-tropospheric troughs. *Mon. Wea. Rev.* **129**, 2570–2584.

Higgins, R. W. and Shi, W. 2005. Relationships between Gulf of California moisture surges and tropical cyclones in the eastern Pacific basin. *J. Climate*. **18**, 4601–4620.

Ho, C.-H., Baik, J.-J., Kim, J.-H., Gong, D.-Y. and Sui, C.-H. 2004. Interdecadal changes in summertime typhoon tracks. *J. Climate*. **17**, 1767–1776.

Hong, S.-Y. 1992. *Numerical simulation of a heavy rainfall event over Korea*. Ph.D. dissertation, Seoul National University, 246 pp. (In Korean with English abstract).

Hong, S.-Y. and Lee, J.-W. 2009. Assessment of the WRF model in reproducing a flash-flood heavy rainfall event over Korea. *Atmos. Res.* **93**, 818–831.

Hwang, S.-O. and Lee, D.-K. 1993. A study on the relationship between heavy rainfall and associated low-level jets in the Korean peninsula. *J. Korean Meteorol. Soc.* 29, 133–146. (In Korean with English abstract).

Keyser, D., Pecnick, M. J. and Shapiro, M. A. 1986. Diagnosis of the role of vertical deformation in a two-dimensional primitive equation model of upper-level frontogenesis. *J. Atmos. Sci.* **43**, 839–850.

Kim, K.-H. 2004. *The role of tropical cyclone in southern China in heavy rainfall formation over the Korean peninsula*. M.S. thesis, Yonsei University, 74 pp.

Kim, J.-H., Ho, C.-H., Kim, H.-S., Sui, C.-H. and Park, S. K. 2008. Systematic variation of summertime tropical cyclone activity in the western north pacific in relation to the Madden–Julian oscillation. *J. Climate*. **21**, 1171–1191.

Lee, J.-W. 2008. *A Numerical study of heavy rainfall occurred in central Korea on 12 July 2006*. M.S. thesis, Yonsei University, 67 pp.

Lee, T.-Y. and Kim, Y.-H. 2007. Heavy precipitation systems over the Korean peninsula and their classification. *J. Korean Meteorol. Soc.* **43**, 367–396.

Lee, D.-K., Kim, H.-R. and Hong, S.-Y. 1998. Heavy rainfall over Korea during 1980–1990. *Korean J. of Atmos. Sci.* **1**, 32–50.

Matyas, C. J. 2010. Associations between the size of hurricane rain fields at landfall and their surrounding environments. *Meteor. Atmos. Phys.* **106**, 135–148.

McBride, J. L. and Zehr, R. 1981. Observational analysis of tropical cyclone formation. Part II: comparison of nondeveloping versus developing systems. *J. Atmos. Sci.* **38**, 1132–1151.

Milrad, S. M., Atallah, E. H. and Gyakum, J. R. 2009. Dynamical and precipitation structures of poleward-moving tropical cyclones in eastern Canada, 1979–2005. *Mon. Wea. Rev.* **137**, 836–851.

Murata, A. 2009. A mechanism for heavy precipitation over the Kii peninsula accompanying typhoon Meari (2004). *J. Meteorol. Soc. Jpn.* **87**, 101–117.

Nakano, M., Kanada, S. and Kato, T. 2010. Statistical analysis of simulated direct and indirect precipitation associated with typhoons around Japan using a cloud-system resolving model. *Hydrol. Res. Lett.* **4**, 6–10.

Ninomiya, K. and Akiyama, T. 1992. Multi-scale features of Baiu, the summer monsoon over Japan and the East Asia. *J. Meteorol. Soc. Jpn.* **70**, 467–495.

Onogi, K., Tslttsui, J., Koide, H., Sakamoto, M., Kobayashi, S. and co-authors. 2007. The JRA-25 reanalysis. *J. Meteorol. Soc. Jpn.* 85, 369–432.

Park, S.-U., Joung, C.-H., Kim, S.-S., Lee, D.-K., Yoon, S.-C. and co-authors. 1986. Synoptic-scale features of the heavy rainfall occurred over Korea during 1–3 September 1984. *J. Korean Meteorol. Soc.* 22, 42–81.

Pierce, C. H. 1939. The meteorological history of the New England hurricane of Sept. 21, 1938. *Mon. Wea. Rev.* **67**, 237–285.

Ritchie, E. A., Wood, K. M., Gutzler, D. S. and White, S. R. 2011. The influence of eastern Pacific tropical cyclone remnants on the southwestern United States. *Mon. Wea. Rev.* **139**, 192–210.

Ross, R. J. and Kurihara, Y. 1995. A numerical study on influences of Hurricane Gloria (1985) on the environment. *Mon. Wea. Rev.* **123**, 332–346.

Schumacher, R. S., Galarneau, T. J. and Bosart, L. F. 2011. Distant effects of a recurving tropical cyclone on rainfall in a midlatitude convective system: a high-impact predecessor rain event. *Mon. Wea. Rev.* **139**, 650–667.

Shim, J.-K. and Hong, S.-Y. 2003. A study of tropical cyclones recurvature and associated momentum transports. *J. Korean Meteorol. Soc.* 39, 59–78. (In Korean with English abstract).

Shin, C.-S. and Lee, T.-Y. 2005. Development mechanisms for the heavy rainfalls of 6–7 August 2002 over the middle of the Korean peninsula. *J. Meteorol. Soc. Jpn.* **83**, 683–709.

Stohl, A., Forster, C. and Sodemann, H. 2008. Remote sources of water vapor forming precipitation on the Norwegian west coast at 60°N – a tale of hurricanes and an atmospheric river. *J. Geophys. Res.* 113, D05102, doi:10.1029/2007JD009006.

Sun, J. and Lee, T.-Y. 2002. A numerical study of an intense quasi-stationary convection band over the Korean Peninsula. *J. Meteorol. Soc. Jpn.* **80**, 1221–1245.

van Zomeren, J. and van Delden, A. 2007. Vertically integrated moisture flux convergence as a predictor of thunderstorms. *Atmos. Res.* **83**, 435–445.

Wang, Y., Wang, Y. and Fudeyasu, H. 2009. The role of Typhoon Songda (2004) in producing distantly located heavy rainfall in Japan. *Mon. Wea. Rev.* **137**, 3699–3716.

Waylen, P. R. and Harrison, M. J. 2005. The coincidence of daily rainfall events in Liberia, Costa Rica and tropical cyclones in the Caribbean basin. *Int. J. Climatol.* **25**, 1665–1674.